Applied Catalysis B: Environmental 152–153 (2014) 250–261

Contents lists available at ScienceDirect

Applied Catalysis B: Environmental

journal homepage: www.elsevier.com/locate/apcatb

Chemical and physical behavior of $CoFe_2O_4$ in steam–iron process with methanol

Stefano Cocchi [a], Massimiliano Mari [a], Fabrizio Cavani [a,b,**], Jean-Marc M. Millet [c,*]

[a] Dipartimento di Chimica Industriale "Toso Montanari", Università di Bologna, Viale Risorgimento 4, 40136 Bologna, Italy
[b] Consorzio INSTM, Research Unit of Bologna, Florence, Italy
[c] Institut de Recherches sur la Catalyse et l'Environnement de Lyon, IRCELYON, UMR 5256 CNRS—Université Claude-Bernard Lyon 1, 2 Avenue A. Einstein, F-69626 Villeurbanne Cedex, France

ARTICLE INFO

Article history:
Received 1 October 2013
Received in revised form 14 January 2014
Accepted 20 January 2014
Available online 27 January 2014

Keywords:
Steam–iron process
Hydrogen production
Methanol reforming
Chemical looping
Mössbauer spectroscopy

ABSTRACT

In this paper we report on the use of $CoFe_2O_4$ spinel for the chemical loop processing for hydrogen production from methanol as the reducing species. The process is based on two steps: (i) the reduction of the spinel carried out with an organic fuel, with generation of a stream containing CO, CO_2, H_2O, and H_2, followed by (ii) the recovery of the original material oxidation state by means of a re-oxidation with water, which leads to hydrogen production. Results of characterization carried out by Mössbauer spectroscopy and X-ray diffraction on the material as-synthesized and at different reduction degrees, and results of reactivity experiments during each one of the mentioned steps, are reported and put into perspective. We found that the complete recovery of the initial oxidation state was indeed not possible with only water, and a third step, with the partial re-oxidation of the material with air was needed for a completion of the cycle.

1. Introduction

Alcohols, especially methanol and ethanol, are promising feeds for hydrogen production due to their high hydrogen-to-carbon atomic ratios, easy handling, and biomass-derivability [1]. Compared to other fuels, methanol has the advantage of producing low amounts of CO during reforming, much less than other fuels. Moreover, the absence of a strong C–C bond fosters reforming at low temperatures (200–300 °C), and limits coke formation; lastly, methanol is biodegradable and liquid in atmospheric conditions. These peculiarities make methanol an interesting hydrogen-carrier fuel not only for portable and small power applications (e.g. for PEM fuel-cells), but also for larger applications. For these reasons, methanol steam reforming (MSR) for hydrogen production continues to be an active area of research [2–5].

One alternative approach used in reforming is the so-called chemical loop; the technical bases for this approach are the thermochemical (cycled) processes, where the heat needed to carry out the endothermic chemical reactions can be provided by solar concentrating energy systems (e.g. such as central power tower, parabolic disk, and double concentration systems) [6,7]. The use of solar energy has been tested for processes such as (a) gasification of coal [8], (b) two-step thermochemical natural gas reforming using metal oxide as an oxidant [9–13], and (c) steam reforming of methane [14,15].

In the chemical-loop approach, the principle is analogous to that used in the old steam–iron process, which was discussed by researchers of the Gas Technology Institute [16]. The steam–iron process used to produce hydrogen in the early 20th century [17] consisted of reacting hot metallic iron with water. Later on, a second step was introduced to recover the original oxidation state of iron, in order to make the process cyclic and competitive with the steam-reforming process, which was introduced during the same period. The steam–iron process had been used in the early 1900s for the production of H_2 in the temperature range 750–850 °C [18]; such high operating temperatures were needed because of the use of cheap, but poorly reactive iron oxide ores. These processes were then abandoned due to the degradation of the iron oxide ores after a few cycles. Recently, however, new interest has been demonstrated in the steam iron process, because of its potential for the production of pure H_2 for fuel cell applications, and because it may serve as a simple, safe, and environmentally benign method for hydrogen storage and/or purification. In the 1970s, a similar cycle was proposed in which, however, the first step consisted of heating the solid material at a very high temperature [19]; in this case, the research on the thermochemical water splitting was focused on lowering the temperature needed for self-reduction of the solid.

* Corresponding authors at: CNRS, 2 Avenue A. Einstein, Villeurbanne, France. Tel.: +33 472445317; fax: +33 472445399.
** Corresponding author.
E-mail addresses: fabrizio.cavani@unibo.it (F. Cavani), jean-marc.millet@ircelyon.univ-lyon1.fr (J.-M.M. Millet).

0926-3373/$ – see front matter © 2014 Elsevier B.V. All rights reserved.
http://dx.doi.org/10.1016/j.apcatb.2014.01.040

In the first stage of the steam–iron process, steam and air react with carbonaceous materials such as coal and biomass to produce a gas mixture of CO, CO_2 and H_2; this mixture is then used to reduce Fe_3O_4 to FeO and Fe. In the second stage, the reduced FeO and Fe are oxidized with steam to Fe_3O_4; water is reduced to H_2, and a hydrogen-rich gas is produced. That means, in practice, a pseudo-storage of hydrogen and its recovery by the redox conversion of iron oxide. The overall reforming process is endothermal, and the energy required to make the process self-sustained can be delivered by adding an exothermal oxidation step of the reduced solid by means of air: this entails using a fraction of the potentially produced hydrogen as a sacrificial fuel. This approach is used in the loop methane reforming process developed by ENI SpA company [20,21].

The main advantage of this two-step process is the relative simplicity of the process design. The second step, oxidation, results in the formation of hydrogen and no difficult or expensive separation steps are required since hydrogen produced is essentially CO-free. Several technical solutions have been proposed over the past 20 years for cycled approaches for both onboard use on vehicles and larger-scale hydrogen plants. They differ in the type of reducing agent used (either methane, CO/H_2 from gasified coal or biomass (CWGS), or even in-situ produced from pyrolysis oil, or hydrogen itself) as well as in the characteristics of the metal oxide used as the electrons/O^{2-} carrier. Iron oxide is generally the material of choice, however, Ge and In oxides are also possible candidate materials [22–44]. Thermodynamic studies demonstrate that the combined Fe_3O_4- or ZnO-reduction and CH_4-reforming process are thermodynamically and kinetically advantageous at temperatures >1000 °C [45,46]. However, the reduced metal may suffer from thermal sintering at such a high temperature. Additives are aimed at limiting sintering phenomena and promoting the oxide reduction and re-oxidation by water; furthermore, the role of supports has been investigated. Kodama et al. [11] studied various redox systems for two-step thermochemical methane reforming: WO_3/W, In_2O_3/In, SnO_2/Sn, V_2O_5/V, MoO_3/Mo, Fe_3O_4/Fe. Lastly, iron-based oxides of Ni-, Zn-, Cu- and Co-ferrites, also supported on zirconia and ceria, proved to be efficient candidates for the reaction [47–50].

In general, mixed ferrites AFe_2O_4 have been widely studied because of the possibility of establishing relationships between chemical–physical features and redox behaviors. Cobalt iron mixed oxide can be considered as one of the most interesting candidate for the steam-iron process because of the higher reducibility if compared to Fe_2O_3, that implies a possible lowering of the temperature of reduction [6,51]. Recently, spinel $CoFe_2O_4$ was also reported for the chemical looping hydrogen process using syngas as the reducing agent [52], showing advantages compared to magnetite during the reduction step, in terms of higher conversion of the reducing agent. Furthermore, we investigated in a previous paper how the crystallinity of the $CoFe_2O_4$ spinel affects the reactivity behavior during the anaerobic oxidation of methanol, which is the first step of a possible chemical-loop reforming using methanol as the reducing substrate [51]; reactivity tests on similar ferrite materials have already been reported, using CH_4 as the reducing fuel [47].

The aim of the present paper is to study (i) the use of $CoFe_2O_4$ for the chemical-loop methanol reforming process, (ii) the structural changes that it undergoes during the interaction with methanol and (iii) how these changes affect the reactivity behavior during the chemical loop, which is carried out by alternating methanol and water feeds. Moreover, one further aim is that of finding conditions at which the initial characteristics of the solid can be restored during use through the redox steps, so allowing repeated cycles with minimal deactivation. The choice of methanol as the reducing agent is driven by both the aim of investigating methanol as the vector for hydrogen production, and the advantage of a complete analysis of the reaction products formed during methanol anaerobic oxidation and decomposition.

2. Experimental

The preparation of the $CoFe_2O_4$ mixed oxides with the inverse spinel structure was carried out as previously described [53]. Briefly, a mixed Co/Fe oxohydrate was co-precipitated by dropping an aqueous solution of Fe (1.0 M) and Co (0.5 M) nitrates into an aqueous solution of NaOH (0.8 M) at 40 °C, while keeping the pH 11 by NaOH-controlled addition. The amount of non-precipitated Co and Fe in the solution was found to be negligible (less that 0.2% of the initial metal used), as highlighted by means of X-Ray Fluorescence (XRF) analysis of the liquid, after separation of the precipitate. Then the solid was vacuum-filtrated, washed with abundant water 3 times to remove Na^+ and nitrates (in overall, ca 1 L of demineralized water was used per gram of precipitate), and dried overnight in air at 120 °C (sample CFp). The solid was analyzed after calcination by means of XRF to check for the residual Na content; the latter turned out to be equal to 0.15 wt% Na_2O.

After the synthesis, the material was calcined in air for 2 h at either 450 °C (sample CF450) or 750 °C (sample CF750). In the course of the study the solids have been characterized after reduction by methanol for various times and temperatures and in some cases further re-oxidized with water for various times and temperatures. In some cases, the treatment parameters have been added to the sample's name. For example, C450-1 h 300-1 h 450 corresponded to a solid prepared at 450 °C, reduced for 1 h at 300 °C and re-oxidized for 1 h at 450 °C.

The crystalline structure of the $CoFe_2O_4$ were obtained by X-ray diffraction (XRD) using a Philips PW 1820 powder diffractometer operating at 40 kV and 40 mA, with Ni-filtered Cu K_α radiation (λ = 1.5418 Å). Crystallite sizes were calculated from XRD peak broadening using the Scherrer equation. Surface areas were determined using a Sorpty 1700 Carlo Erba instrument, based on the BET single point method (N_2 adsorption at the temperature of liquid N_2). Relative errors on both types of obtained values were calculated by repeating measurements on several samples, each one freshly prepared.

Mössbauer spectroscopy was used to analyze the characteristics of iron atoms in the fresh, used, and re-oxidized cobalt ferrite samples. The Mössbauer spectrometer was a home made apparatus described elsewhere [54]. Both a ^{57}Co/Rh γ-ray source and a conventional constant acceleration Mössbauer spectrometer were used for spectra collection. Isomer shifts were given with respect to α-Fe. All spectra were taken at room temperature and ambient atmosphere; samples were diluted in sucrose at about 50%$_w$ concentration. Integrated areas under individual deconvoluted peaks were used to obtain the relative populations of different iron species, assuming an equal recoil-free fraction for all iron species. The parameters characterizing a Mössbauer spectrum were determined by least-squares fitting and minimizing the χ^2 quadratic function:

$$\chi^2 = \sum_i \frac{(y_i \mathrm{th} - y_i \exp)^2}{y_i \exp} \times \frac{1}{N-K} \quad (1)$$

where N is the number of measured points, K the number of the parameters to be determined, y_i exp and th, respectively, measured and calculated spectral values in velocity for each point i. The calculations were made using pure Lorentzian functions.

Reactivity experiments were carried out by loading 400 mg of samples shaped into particles with diameters ranging from 0.25 to 0.6 mm, in a fixed-bed quartz flow reactor. Before testing, the catalysts were pretreated in a N_2 flow at 450 °C for 2 h in order to decompose adsorbed carbonates. The catalytic bed temperature

was measured by means of an in-set axial thermocouple. The reaction was carried out by continuously feeding a stream of methanol vapors (15.6 mol%) and N_2; N_2 was also used as an internal standard. Contact time was 0.25 s. The reaction time was maintained long enough to reach the maximum level of solid reduction that could be obtained under those reaction conditions. Re-oxidation experiments were carried out by feeding a steam-containing stream (19% steam in N_2) over the pre-reduced solid; the contact time used for these experiments was 0.25 s. Yields of each C-containing product were calculated by referring the outlet molar flow of each reaction product to the inlet molar flow of methanol. In the case of H_2 and H_2O yields, the outlet molar yields were also referred to the inlet flow of methanol, dividing the obtained values by 2. As the solid released oxygen to form products until the complete reduction was achieved, and due to the fact that carbonaceous residues may accumulate on the solid during reaction, calculation of an atomic balance on O atom or on C atom was not possible. Therefore, we carried out an atomic balance on H (the only species which was not contained in an accumulation term in material balances for the flow reactor), which made it possible to calculate: (a) the instantaneous balance on C and thus the amount of C accumulating on the catalyst (expressed with the term "carbon"), and (b) the instantaneous balance on O and thus the amount of O released from the catalyst. The latter value made it possible to calculate the reduction degree of the solid during the reactivity test. The integration of instantaneous values of product yields and methanol conversion from zero time until a defined value of reaction time enabled to calculate the overall corresponding "integral yields and conversion". Samples for XRD analysis and Mössabuer ex-situ spectroscopy were prepared by carrying out methanol reduction and/or water re-oxidation tests using a residence time equal to 1.25 s.

An Agilent 3000A micro-GC was installed on-line to monitor the concentration of each component in the effluent stream. This instrument was equipped with 3 columns: (a) a Plot Q column, carrier N_2, for the separation of CH_4, CO_2, H_2O and methanol; (b) a OV1 column, carrier N_2, for the separation of CO_2, formaldehyde, H_2O, methanol, methyl formate, dimethyl ether, dimethoxymethane; (c) a Molecular Sieve 5A column, carrier Ar, for the separation of H_2, O_2, N_2, CH_4, and CO. Plot U backflash column was installed to avoid CO_2 and H_2O poisoning in the third column.

3. Results and discussion

3.1. Characterization of as-synthesized oxides

The characterization of the morphology of fresh and calcined $CoFe_2O_4$ ferrite is presented on Table 1. A spinel-type oxide was obtained in all cases and a significant sintering of particles was observed with increasing annealing temperature.

Synthesized materials were characterized by means of XRD, as described in detail in Ref. [51]; in all cases, the spinel-like oxide was the only crystalline phase detected. The Mössbauer spectra of the corresponding samples are presented in Fig. 1. Mössbauer spectroscopy is a very sensitive analyzer of iron chemical–physical properties, specially when applied to doped magnetites or ferrites [55–59]; resulting spectra are not influenced only by the morphological features of the material or the oxidation state of iron ions,

Table 1
Specific surface area (SSA) and crystallite size (from Scherrer equation) of fresh samples.

Sample	Sample's treatment	SSA ($m^2\ g^{-1}$)	Crystallite size (nm)
CFp	Dried at 120 °C	180	–
CF450	Calcined at 450 °C	70 ± 14	15 ± 2
CF750	Calcined at 750 °C	9 ± 2	41 ± 9

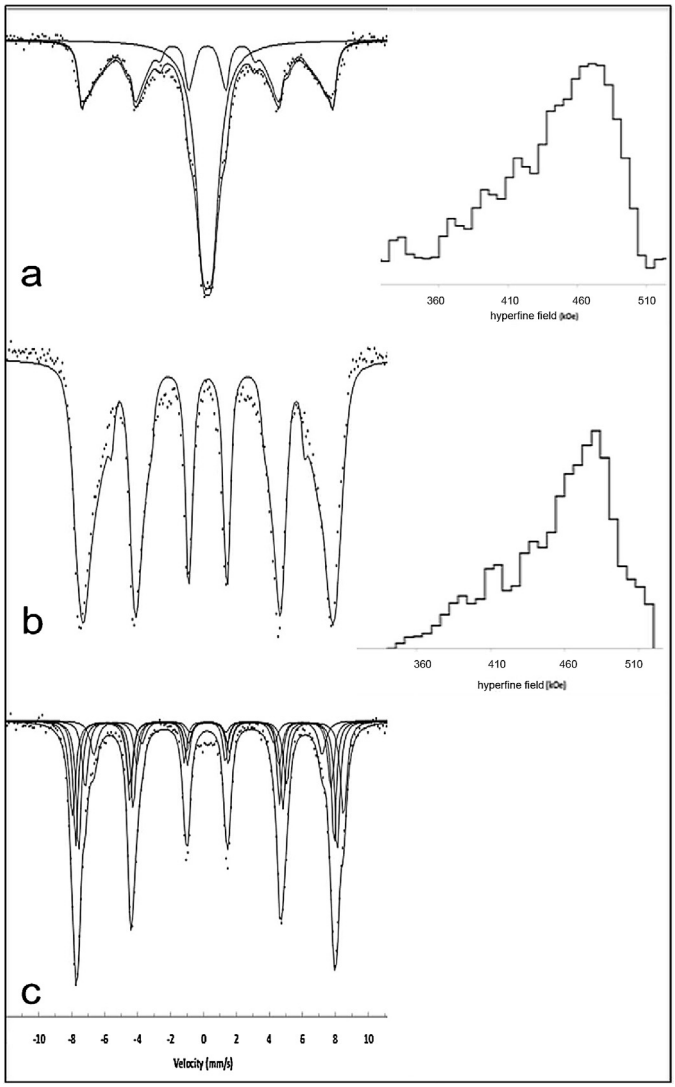

Fig. 1. Left: Mössbauer spectra recorded at room temperature for $CoFe_2O_4$ samples: fresh, CFp (a), calcined at 450 °C, CF450 (b) and 750 °C, CF750 (c). Solid lines are derived from least-square fits. Right: hyperfine field histogram accounting for the magnetic sextet distribution.

but also by the internal magnetic field, which is created by the different ion distribution in the neighboring positions. In accordance with Sawatzky et al. [58,59], typical crystalline mixed ferrite spectra can be fitted considering at least five sextets, each corresponding to a given environment for the ferric cations. These five different environments have been explained by the inverse spinel configuration of $CoFe_2O_4$, where half of octahedral sites are occupied by Co^{2+} cations and the other half by Fe^{3+} ones. On the other hand, tetrahedral sites are completely filled by Fe^{3+} in the so-called high-spin field distribution.

The general formula is:

$$\left(Co^{II}_{1-\delta}Fe^{III}_{\delta}\right)_{Th}\left(Fe^{III}_{2-\delta}Co^{II}_{\delta}\right)_{Oh}O_4 \quad \text{with} \quad 0 < \delta < 1 \qquad (2)$$

where δ is the inversion degree of the oxide.

Experimentally, a high inversion degree is usually obtained with an annealing treatment followed by a slow cooling ramp, but complete inversion is rarely observed. Consequently, the nature of atoms in A (Th) and B (Oh) sites affects the internal magnetic field depending on the chemical composition of the unit cells. Only six tetrahedral nearest neighbors surround octahedral sites, so the composition of the Oh environment is significant in the

Table 2
Mössbauer parameters calculated from the spectra of CF750 sample, recorded at 25 °C.

Site A			Site B1			Site B2			Site B3			Site B4			δ
IS	H	I	IS	H	I	IS	H	I	IS	H	I	IS	H	I	
0.18	48.4	24	0.37	50.8	24	0.37	48.5	26	0.37	46.1	16	0.37	42.8	10	48
0.19	48.2	35	0.40	50.9	21	0.40	48.5	21	0.40	46.1	13	0.40	42.9	10	70
0.20	48.4	39	0.41	50.9	20	0.41	48.5	19	0.41	46.0	13	0.41	43.0	9	78
0.20	48.1	45	0.43	51.0	18	0.43	48.5	17	0.43	46.0	10	0.43	43.0	10	90

IS: isomer shift (mm s^{-1}), *H*: internal magnetic field (T), *I* relative spectral area (%); δ: inversion degree of the spinel; quadrupole splittings were fixed to zero.

total magnetic field. On the other hand, the iron ions in tetrahedral sites are surrounded by 12 octahedral positions and the chemical composition of these sites only marginally affects the internal magnetic field. Therefore, one out the five components in the fitting is referred to iron atoms in tetrahedral positions, while the other four components are referred to Fe^{3+} in octahedral sites, with a different chemical composition of the surrounding atoms: this interpretation is the so-called "next–nearest neighbors' theory". As for the magnetite (Fe_3O_4), the fitting of spectra may be obtained considering only two different species of iron: Fe^{3+} and $Fe^{2.5+}$: as in the above case, the structure of the spinel is inverse, and therefore the former is referred to the trivalent iron cation in tetrahedral position, while the latter is a species that derives from the electron hopping between Fe^{2+} and Fe^{3+} in octahedral positions, in accordance with Sawatzky et al. [60].

Coming back to the results in Fig. 1, it can be seen that the spectra of the three samples were quite different. CFp showed the presence of two components in the fitting curve: a doublet and a sextet. The doublet component was due to the super-paramagnetic behavior of the sample, which is a consequence of the small dimension of the particles; magnetization randomly changes under the effect of the temperature, and only the effect of the electric field gradient at the nucleus is observed, which gives rise to a doublet in the total spectra. Isomer shift (IS) and quadrupole splitting (QS) were, respectively, equal to 0.33 and 0.69 mm s^{-1}, values that are in agreement with other authors [61–63]. In addition to the doublet, a distribution of sextets was needed to fit the total spectrum that derived from the larger ferromagnetic particles. The hyperfine fields distribution with a maximum around 42 T, is also shown in Fig. 1. Both sub-spectra contributed for about 50% of the total fitting, if similar *f*-factor was assumed for the two components. In CF450, the mid-temperature annealing (450 °C) led to a sintering that enabled to observe superparamagnetic particles but still to an incomplete crystallization of the oxide, needing a distribution of internal magnetic fields for fitting the spectrum. Obviously, the lack of resolution of the magnetic hyperfine structure prevents from a clear quantitative description in terms of both tetrahedral and octahedral Fe sites.

CF750 is the most well-crystallized compound and its spectrum was well fitted with the five sextets proposed in the literature. Furthermore, in the present work the fitting has been made using the same isomer shift for the iron species in octahedral sites, in order to reduce the number of parameters in the fitting. This was required because a very high number of freedom degrees could lead to calculated values with no chemical–physical meaning. However different isomer shifts were assumed and fixed for B sites. The hyperfine parameters corresponding to the best fit, i.e. the one with the lower χ^2 value, are reported in Table 2. The relative ratios of B sites derived from relative spectral areas were in agreement with the probability distribution to find a Fe^{3+} in B site with *m*Fe^{3+} in their next–near environment, which is defined by the equation:

$$P(m) = \frac{6!}{m!(6-m)!} \times \delta^m (1-\delta)^{6-m} \quad (3)$$

where *m* is the number of the surrounding Fe^{3+} and δ is the inversion degree of the spinel. For 78% of inversion, the values reported in Table 3 have been calculated; they were in good agreement with those obtained by Ferreira et al. on cobalt ferrite similarly prepared [64].

3.2. Reactivity experiments

Fig. 2 shows the values of methanol conversion and the corresponding selectivity to each product (the latter calculated taking the instantaneous yield of that compound into account) plotted in function of the extent of solid reduction (see Section 2 for a description of the method used to calculate the reduction degree); moreover, the time needed to reach the corresponding reduction degree is also shown.

Samples CF450 and CF750 were used for these experiments (Fig. 2 top, reduction at 300 °C of CF450; Fig. 2 middle, reduction at 300 °C of CF750; Fig. 2 bottom, reduction at 420 °C, of CF450). The results shown are extrapolated from the reactivity behavior previously reported [51]; the plot shown is useful in the aim of correlating the ex-situ characterization of samples (reported below) with the reactivity behavior shown and the calculated degree of reduction. It is shown that both the conversion of methanol and the selectivity to products were strongly affected by the reduction degree, as well as by the temperature at which the reduction was carried out. As discussed in a previous paper, different reaction areas were distinguished with regard to product yields at 300 °C; hereafter we describe briefly the main results of reactivity experiments [51].

As shown in Fig. 2 (top), at the beginning of the reduction step (time interval approx. 0–22 min, at 300 °C), when the solid is still oxidized, the reactions registered were methanol partial oxidation to CO_2/H_2 and methanol decomposition to CO/H_2, with also formation of traces of formaldehyde and other derived products. Coke also formed from the very beginning of the reaction time, but it showed a decreasing trend during this first period. At the end of this first-zone, the reduction degree of the solid material was ca. 3.5%.

During a second period of reaction (time approx. 22–100 min), a rapid rise of CO and H_2 formation was observed, both compounds being formed by methanol decomposition, due to the increasing extent of ferrite reduction; at that step, the formation of coke became considerable, and showed an increasing selectivity. At the end of this period, the solid was reduced by the 20% of the complete

Table 3
Calculated statistical distribution of Fe^{3+} in B octahedral sites, for the CF750 sample.

Site	M	*P*(m)	Relative content (%)
B1	6	22.5	33
B2	5	38.1	31
B3	4	26.9	21
	3	10.1	
B4	2	2.14	15
	1	0.24	

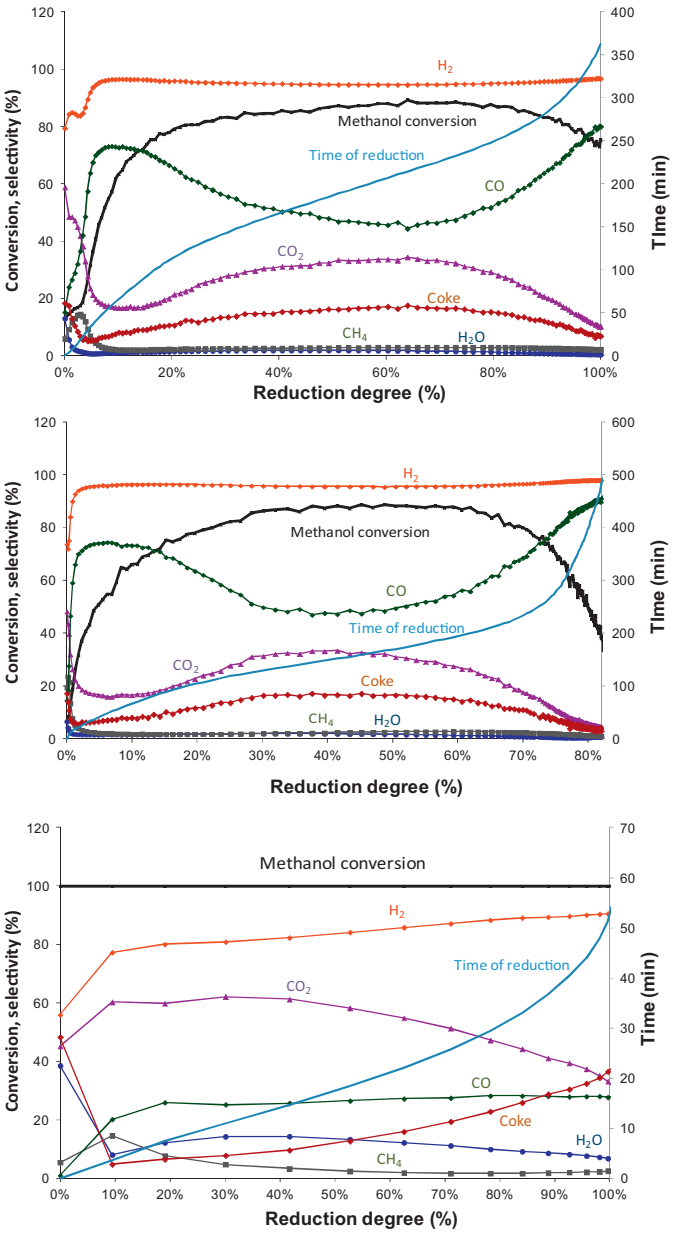

Fig. 2. Methanol conversion, product selectivity as a function of the solid reduction degree, during the reduction (top) at 300 °C of CF450; (middle) at 300 °C of CF750; and (bottom) at 420 °C of CF450.

reduction. Therefore, the presence of reduced sites with dehydrogenating properties justifies the formation of these products.

During a third period (approx. 101–200 min reaction time), an increase of CO_2 generation and a concomitant lower CO production took place showing an important contribution of Boudouard disproportionation. During this period, the solid reached the 60% of the complete reduction. Lastly, the reaction carried out up to the complete reduction of the solid oxide (which at these conditions took about 370 min), with a decreased methanol conversion due to the deactivation of the material, and with a nearly complete selectivity into CO and H_2. Conversion of methanol at the end of the catalyst reduction still was over 70%, because of the high catalytic activity of the completely reduced material in methanol decomposition.

The behavior shown by sample CF750 at 300 °C was similar to that of CF450 (Fig. 2, middle). The initial reaction period, during which the main products were CO_2 and H_2, however lasted only 4 min; therefore it was much shorter than the corresponding initial period of CF450. This was attributed to the fact that in the more crystalline CF750 sample, a lower concentration of highly reactive surface sites was present [51]. Based on the overall extent of reduction evaluated for the two samples during the first reduction period (3.5% after 22 min reaction time for CF450, 0.17% after 4 min reaction time for CF750), this difference could be ascribed not only to the different values of the surface area in the two samples, but also to their distinct reactivity features. The presence of highly reactive (reducible) surface species in CF450 was suggested, and, conversely, these species were less exposed in the case of CF750 and may correspond to surface octahedral (Co^{2+}/Fe^{3+}) sites, which are present in greater amount on the surface of the CF450 sample [51,53]. Furthermore, the reduction rate of CF750 after 6 h reaction time drastically decreased and, for this reason, the reaction was stopped when the solid reduction degree was 82%.

At 420 °C the phenomena observed were similar to those shown at 300 °C, but all variations previously shown occurred much faster, and therefore the four different time-zones took much shorter times to occur; indeed, at this temperature, the maximum level of spinel reduction in CF450 was reached after about only 60 min (Fig. 2). The formation of coke was more significant than it was at 300 °C, and the maximum value of 40% yield was reached after 60 min.

We then carried out the re-oxidation step with steam on pre-reduced samples, in order to assess the possibility of fully recovering the original oxidation state of the oxide; the products during spinel re-oxidation were H_2, CO, and CO_2, which formed according to the following reactions:

$$Me^0 + xH_2O \rightarrow MeO_x + xH_2 \quad (4)$$

$$C + xH_2O \rightarrow CO_x + xH_2 \quad (5)$$

Fig. 3 reports the yields to hydrogen, CO and CO_2 during the re-oxidation carried out at 420 °C, after the pre-reduction of CF450 at

Table 4
Parameters inferred from Mössbauer spectra of CF450 after the reduction step with methanol.

Samples code[a]	Fe^{3+} A site			Fe^{3+} B sites*				$Fe^{2,5+}$			Alloy			Fe_3C			Fe^{3+} doublet		
	IS	H	I	%a	%b	%c	%d	IS	H	I	IS	H	I	IS	H	I	IS	QS	I
CF450-1 h 300	0.17	48.6	21	30	15	9	42	–	–	–	–	–	–	–	–	–	–	–	–
CF450-2 h 300	0.18	48.6	15	21	26	12	6	–	–	–	0.00	33.8	1	0.05	20.0	9	0.32	1.15	10
CF450-1 h 360	0.19	49.3	18	14	24	8	2	0.55	45.0	10	0.00	34.5	14	0.10	20.3	6	0.32	1.17	4
CF450-2 h 360	0.20	48.8	11	14	15	4	1	0.68	44.7	6	−0.01	34.4	28	0.09	20.3	14	0.22	1.66	6
CF450-1 h 420	0.20	49.4	13	7	27	4	1	0.63	46.0	13	0.00	34.2	32	0.00	21.0	2	–	–	–
CF450-2 h 420	0.24	49.0	12	5	5	1	–	0.70	46.0	5	0.00	34.4	42	0.04	20.0	25	–	–	–

IS: isomer shift (mm s^{-1}), H: internal magnetic field (T), I relative spectral area (%), QS: quadrupole splitting (mm s^{-1}).

[a] See Section 2 for details on samples code.

* Isomer shift of 0.37 mm s^{-1} and internal magnetic field of the four components comprised between 51.0 and 43.0 T.

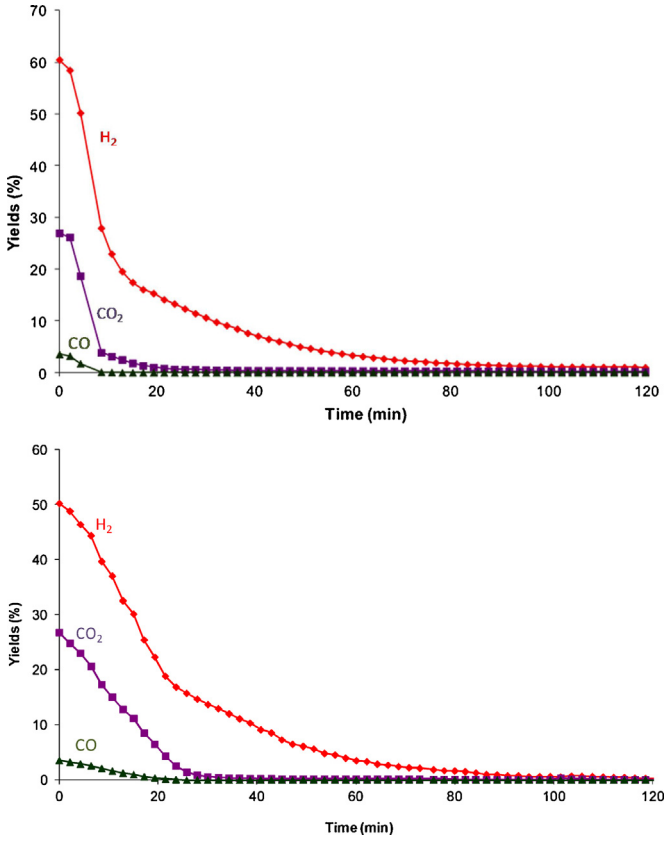

Fig. 3. Yields to CO, CO_2 and H_2 during re-oxidation with water at 420 °C of the CF450 sample pre-reduced at 300 °C (top) and at 420 °C (bottom).

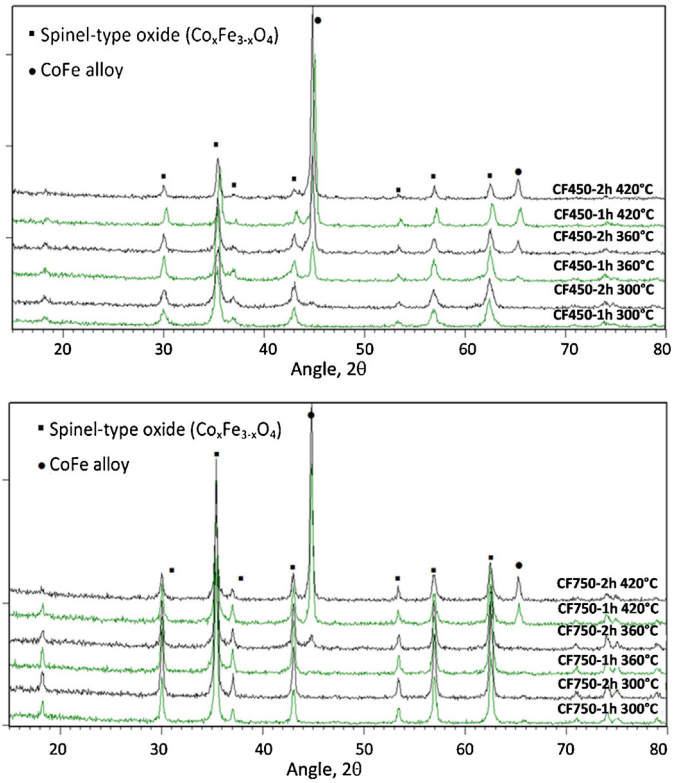

Fig. 4. XRD pattern of samples reduced at different temperatures and for different times (top CF450, bottom CF750).

300 and 420 °C. The re-oxidation step took about 80 min, when no more conversion of H_2O was registered.

3.3. Characterization of oxides after reduction and overall redox steps

The CF450 and CF750 samples were first characterized by XRD and Mössbauer spectroscopy after the reduction step with methanol. Fig. 4 shows the XRD patterns of the samples reduced at different temperatures and for different periods of time. Figs. 5 and 6 show the Mössbauer spectra of the corresponding samples and Tables 4 and 5 gather the hyperfine parameters calculated from these spectra.

The X-ray diffraction patterns showed that the main phase formed after reduction was a CoFe alloy with in minor amount a spinel type phase. No other phases like FeO or CoO were observed. Moreover, patterns show that the reduction of CF450 was deeper, i.e., more rapid than that of CF750, under the same reaction conditions. This difference was more evident at low temperatures (300 and 360 °C) and agreed with the presence of more reactive sites for the less crystalline sample (CF450). At 420 °C, the reduction rate appeared similar for both samples, if compared to the different behaviors shown at 300 °C and 360 °C; however, a higher CF450 reduction rate was still observable: the reflections attributable to the spinel phase in the XRD pattern registered after 2 h reduction time at 420 °C were weaker in CF450, which means a higher conversion degree of the solid material.

In contrast with the corresponding XRD patterns, CF450 Mössbauer spectra showed that some changes had occurred even after 1 h of reaction at 300 °C. Whereas a distribution of internal magnetic field was needed to fit the spectrum of the fresh compound, a fit with the five sextets was possible for the new spectra. This could be ascribed to a change in sample crystallinity, which probably derived from partial reduction of Fe^{3+} in the fully oxidized sample during first contact with methanol. The same effect was shown in regard to reactivity results recorded during the first period of reaction, which was considerably different for the two samples. The main reduced phase identified was a CoFe alloy, as also inferred from the XRD patterns; this alloy was characterized by an internal magnetic field around 35 T. It has been shown that the trend of this

Table 5
Parameters inferred from Mössbauer spectra of CF750 after the reduction step with methanol.

Samples code[a]	Fe^{3+} A site			Fe^{3+} B sites[*]				$Fe^{2,5+}$			Alloy			Fe_3C (%)			Doublet Fe^{3+}		
	IS	H	I	%a	%b	%c	%d	IS	H	I	IS	H	I	H	IS	I	IS	QS	I
CF750-1 h 300	0.18	48.6	26	28	10	7	52	–	–	–	–	–	–	–	–	–	–	–	–
CF750-1 h 360	0.20	48.9	25	31	28	9	4	–	–	–	0	35.7	2	–	–	–	0.31	0.90	1
CF750-2 h 360	0.25	48.7	43	11	19	6	0	0.60	43.8	4	-0.06	34.6	4	204	0.03	7	0.38	1.58	5
CF750-1 h 420	0.20	49.3	16	21	22	5	2	0.62	45.6	5	0.01	34.8	30	–	–	–	–	–	–
CF750-2 h 420	0.19	48.9	12	18	17	4	2	0.80	44.6	1	0.00	34.7	40	204	0.00	5	-	–	–

IS: isomer shift (mm s^{-1}), H: internal magnetic field (T), I relative spectral area (%), QS: quadrupole splitting (mm s^{-1})

[a] See Section 2 for details on samples code.

[*] Isomer shift of 0.37 mm s^{-1} and internal magnetic field of the four components comprised between 51.0 and 43.0 T.

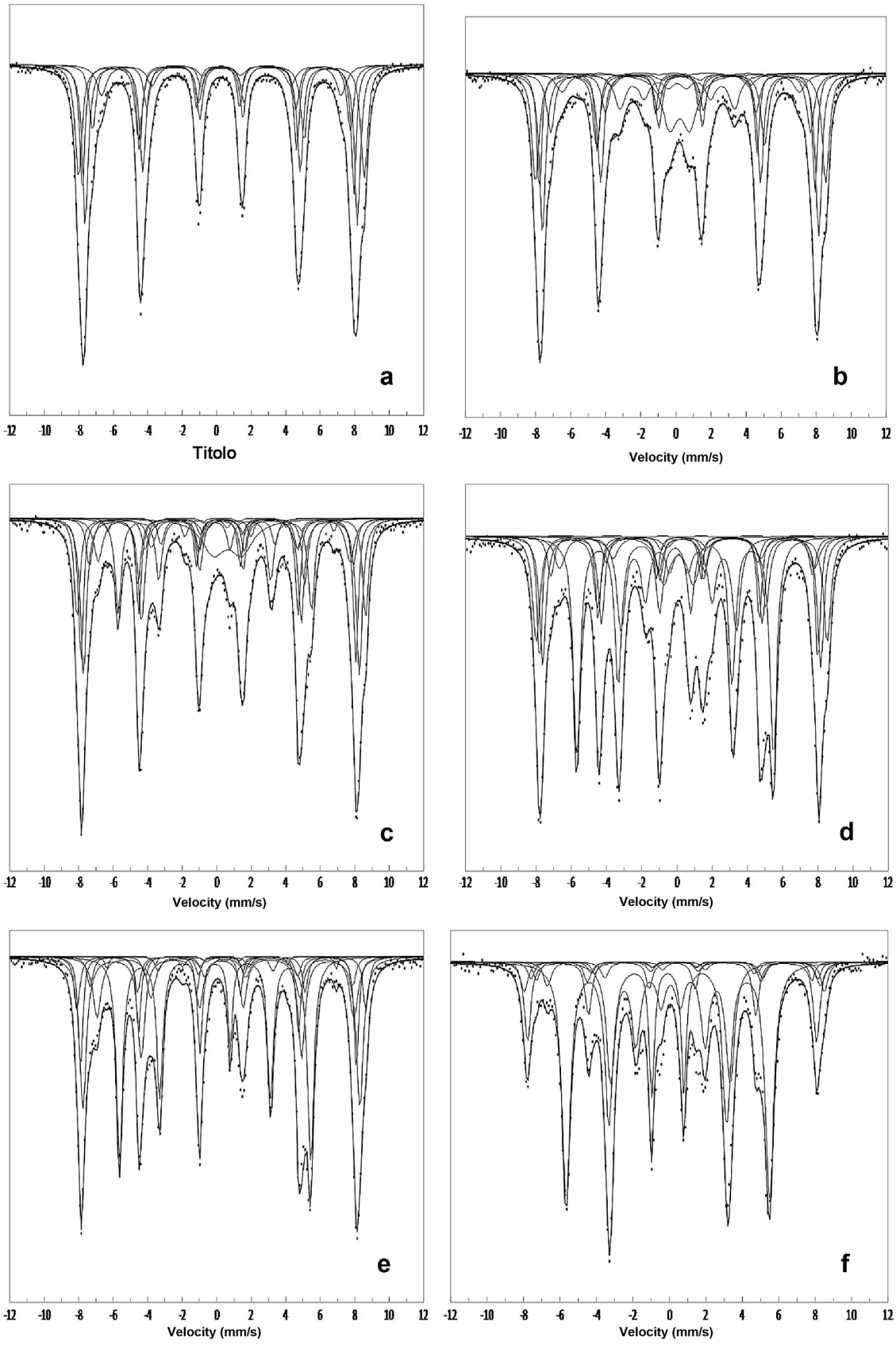

Fig. 5. Mössbauer spectra of CF450 samples after the reduction step with methanol at 300 °C for 1 and 2 h (a and b), at 360 °C for 1 and 2 h (c and d) and at 420 °C for 1 and 2 h (e and f). Solid lines are derived from least-square fits.

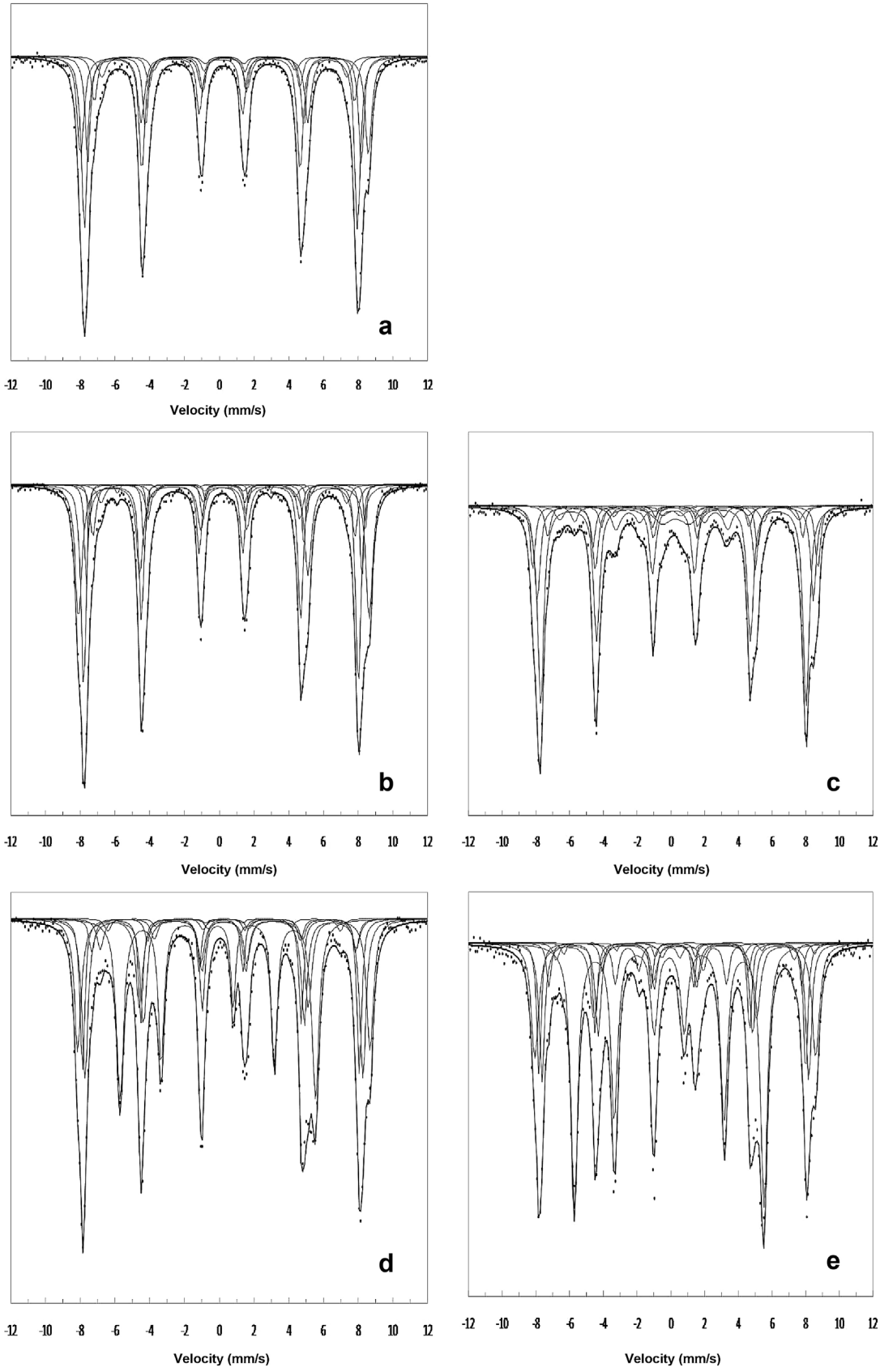

Fig. 6. Mössbauer spectra of CF750 samples after the reduction step with methanol at 300 °C for 1 h (a), at 360 °C for 1 and 2 h (b and c) and at 420 °C for 1 and 2 h (d and e). Solid lines are derived from least-square fits.

hyperfine parameter depends on the composition of the alloy, as described by Johnson et al. [65], and according to the calculated value, the cobalt concentration in the alloy should be around 40%. This suggests that a segregation process was taking place during the reduction step with the formation of a reduced phase richer in Co. The presence of a sextet with an IS of about 0.6 mm s^{-1} ascribed to $Fe^{2.5+}$ species evidenced the formation of a small quantity of Fe_3O_4, that could confirm the occurrence of such segregation. It has to be recalled that Fe_3O_4 cannot be distinguished from the mixed ferrite by XRD. The rapid formation of a CoFe alloy is in agreement with the results of reduction tests registered during the second zone at 300 °C, where the rapid raising of methanol conversion can be finally attributed to the higher activity of metal-type catalytic sites.

Besides the discussed phases, the formation of Fe_3C carbide was detected. The latter should be formed by reaction between CO and iron-reduced species [66–70]. It was found in a non-negligible amount in all the samples after a 3 h reduction; this means that both the reduced iron and the high CO concentration led to the disproportionation of carbon monoxide to iron carbide and CO_2 in all cases; therefore, it is possible to say that this pseudo-Boudouard reaction is leading to the formation of the iron carbide species. The main difference between CF450 and CF750 was finally the ratio between Fe_3C and CoFe alloy, which is lower for CF750. This can be explained by the fact that CF450 has a much higher specific surface area, which promoted the formation of the carbide that takes place at the surface of the compounds.

A total reduction degree of the sample can be obtained from the sum of Fe^0 and carbide species; the analysis showed that a higher reduction degree was reached for CF450 (100% reduction) than for CF750 (82%), further confirming the different behaviors of the two materials. It can be noted that to get the best fits a doublet characterized by an IS of 0.32 mm s^{-1} and a QS of 1.2 mm s^{-1} had to be considered. This doublet corresponded to ferric species, tentatively attributed to a super-paramagnetic ferric oxide phase formed from reduced Fe^0 nanoparticles upon oxidation by air, during the recovery of the samples at room temperature. Their low contribution (<5%) has consequently been added to that of the Fe^0 containing phases for reduction balance calculation. In order to better visualize the results obtained by Mössbauer spectroscopy, Fig. 7 has been drawn, showing the relative amounts of each identified species. It is possible to observe that:

(1) the reduction rate of CF750 was lower than that of CF450, in agreement with XRD results;
(2) the iron carbide-to-CoFe alloy ratio was lower in CF750 than in CF450, presumably because of the lower specific surface area of the former sample;
(3) the presence of Fe_3O_4 as an intermediate compound in the reduction process is evident mainly in CF450, probably because its formation was proportional to the surface area (as it was for the iron carbide species).

However, a role could be played by the different sites exposed, which might show different reactivity in regards to carbide formation.

The CF450 and CF750 samples have also been characterized after re-oxidation by water. The Mössbauer spectra of re-oxidized samples are shown in Fig. 8. The corresponding calculated hyperfine parameters are gathered in Table 6. After one redox cycle, the spectra of the materials were different from the corresponding initial ones (Fig. 1). The presence of only two sextets characterized by an internal magnetic field of about 45.5 and 49 T evidenced the presence of magnetite Fe_3O_4. The two sextets have similar intensities, which means that Fe^{3+} is preferentially >located in octahedral sites, and not equally distributed in both sites as it is in pure Fe_3O_4. This is because the obtained oxide contains cobalt in the octahedral sites,

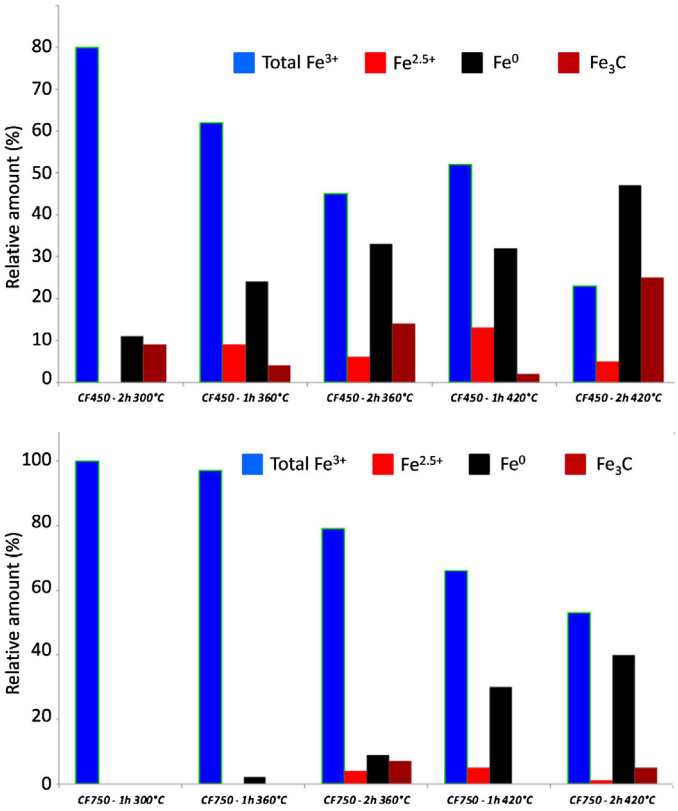

Fig. 7. Nature and relative amounts (%) of the different Fe species present during the reduction of CF450 (top) and CF750 (bottom) samples, as found by means of Mössbauer spectroscopy. Results are arranged considering the conversion of the reactant ($CoFe_2O_4$ spinel, blue columns). (For interpretation of the references to color in this figure legend, the reader is referred to the web version of this article.)

Table 6
Parameters inferred from Mössbauer spectra of pre-reduced and re-oxidized samples.

Samples code[a]	$Fe^{2,5+}$ Oh			Fe^{3+} Th		
	IS	H	I	IS	H	I
CF450-6 h 300-3 h 420	0.62	45.5	49	0.27	48.8	51
CF450-0.5 h 420-3 h 420	0.64	46.0	58	0.25	49.0	42
CF750-6 h 300-3 h 420	0.63	45.9	51	0.26	49.1	49
CF450-0.5 h 420-3 h 420	0.62	45.8	47	0.27	49.2	53

IS: isomer shift (mm s^{-1}), H: internal magnetic field (T), I relative spectral area (%).
[a] See Section 2 for details on samples code.

which derives from the re-oxidation with water of reduced materials, whereas the original oxidation state of the iron atoms was not completely recovered. Therefore, the spinel phase was characterized by the general formula $Co_xFe_{3-x}O_4$, with $0 < x < 1$, which justifies the ratio between the Fe_{Oh} and Fe_{Th}.

Furthermore, by approximating the structure to that of a complete inverse spinel-type oxide, and considering only one sextet as the contribution for the Fe^{3+} in the octahedral sites of the mixed structure, it was possible to estimate a 25% complete recovery of the original oxidation state (Co^{2+} and Fe^{3+}), while 75% of iron species were present as Fe_3O_4. The re-oxidation step with water may be divided into three main reactions: (a) the re-oxidation of the Fe_3C carbide to magnetite, (b) the re-oxidation of the metallic cobalt/iron alloy to an intermediate oxide (where iron has both +2 and +3 oxidation state), and (c) the subsequent oxidation of this intermediate compound into the spinel-type oxide; this third step is a slightly exothermic reversible reaction [19], thermodynamically more favored at a low temperature. This may suggest that

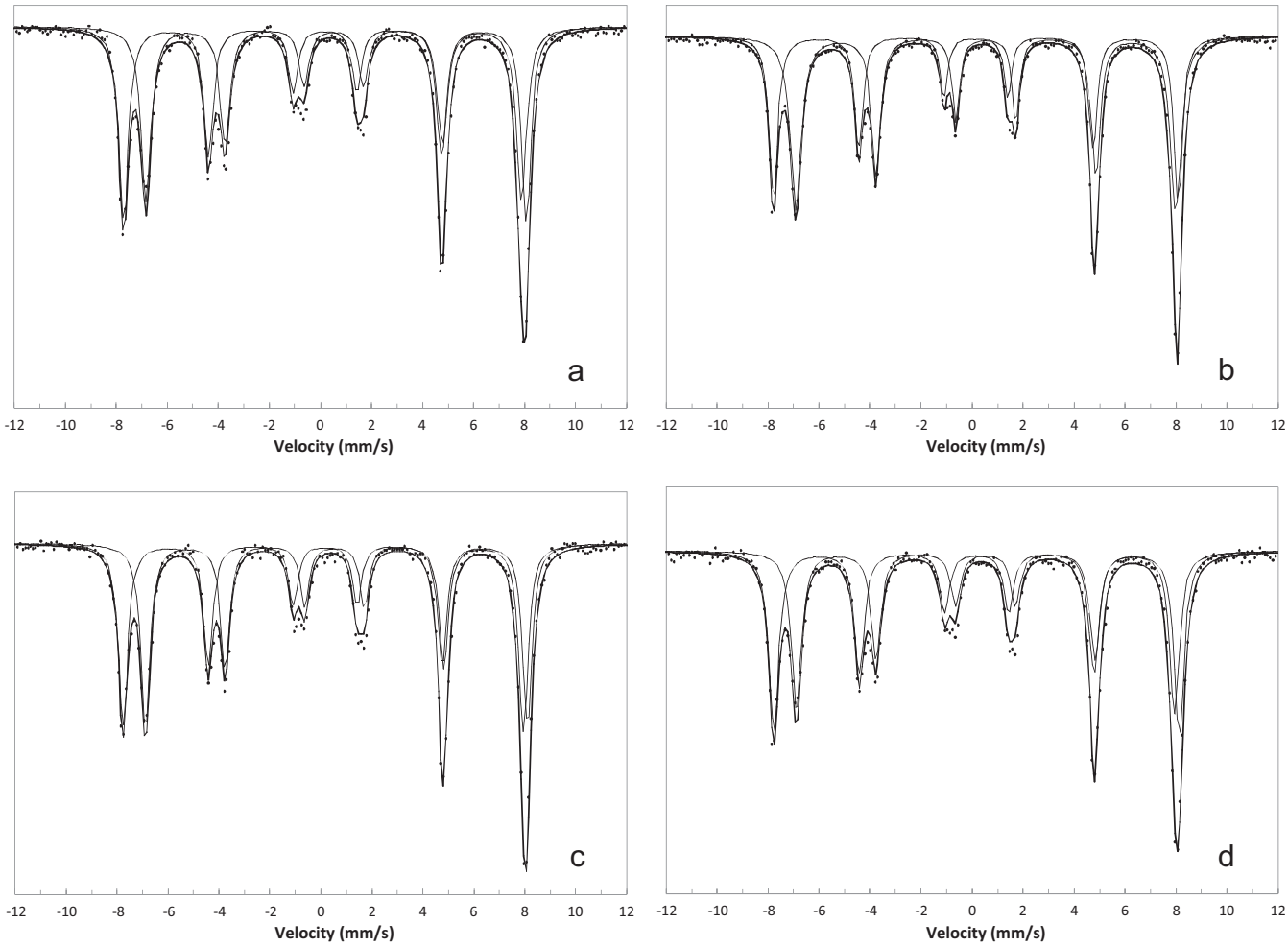

Fig. 8. Mössbauer spectra of CF450 (a and b) and CF750 (c and d) samples after complete reduction and re-oxidation with water. In all cases, re-oxidation was carried out with steam, at 420 °C and contact time 0.2 s. Pre-reduction with methanol was carried out at 300 °C and 0.2 s contact time (a and c), and at 420 °C and 0.2 s contact time (b and d). Solid lines are derived from least-square fits.

the presence of Fe_3O_4 in the exhaust material originates partially from an incomplete re-oxidation, and not only from segregation phenomena.

3.4. Evaluation of a three-step process with two re-oxidations with water and with air

Since the re-oxidation process with water did not allow recovering the starting oxide, we decided to carry out a further step with air; this step was performed at 450 °C in an air flow (20 mL min^{-1}) for 3 h; these experimental conditions were chosen in order to use a similar annealing procedure compared to that one used for the calcination of the spinel. The oxide obtained was analyzed by mean of Mössbauer spectroscopy (Fig. 9 and Table 7) and XRD (Fig. 10). Again it was not possible to conclude on the nature of the phases formed from XRD but the Mössbauer spectrum of the re-calcined sample corresponded well to that of the $CoFe_2O_4$ spinel phase, while Fe_3O_4 was no longer detected. This result confirmed that the re-oxidation step with air was useful for recovering the original oxidation state of the material. Moreover, the step with air could completely re-oxidize the oxide even after a complete reduction step, whereas only 25% of the original spinel

Table 7
Mössbauer parameter of the CF450 sample after reduction with methanol, re-oxidation with steam, and final oxidation with air.

Sample code[a]	Fe^{3+} Th			Fe^{3+} Oh sites			
	IS	H	I	%a	%b	%c	%d
CF450-6 h 300-6 h 420-3 h 450	0.19	48.3	22	27	26	12	13

IS: isomer shift (mm s^{-1}), H: internal magnetic field (T), I relative spectral area (%).
[a] See Section 2 for details on samples code.

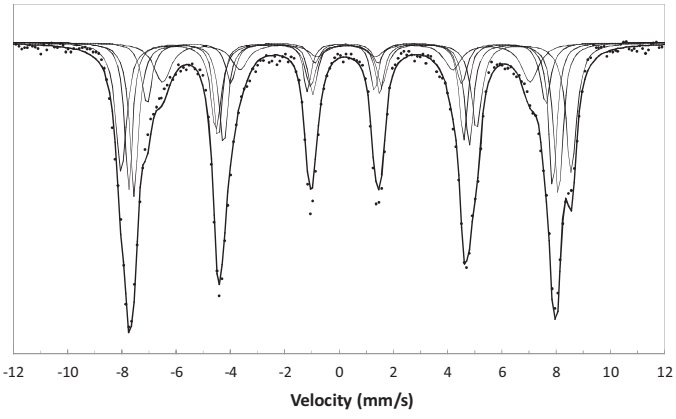

Fig. 9. Mössbauer spectrum of the CF450 sample after pre-reduction with methanol, re-oxidation with steam and final oxidation with air. Solid lines are derived from least-square fits.

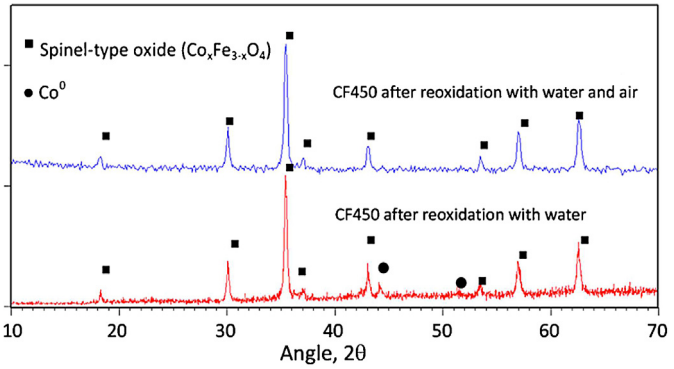

Fig. 10. XRD pattern of used CF450 with two different re-oxidation procedures: (top) with water and then air, (bottom) with water only.

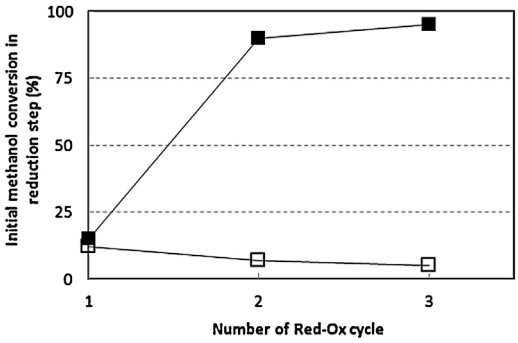

Fig. 12. Initial conversion of methanol in the reducing step of next cycles with a CF450 sample re-oxidized either with water only (■), or with water and then air (□).

composition could be recovered by means of only water re-oxidation.

Finally in order to check whether the two-step re-oxidation (steam plus air) had led to the recovery of the original reactivity of the spinel, we have compared the conversion and yield obtained during reaction with methanol (300 °C, CF450 sample) on two samples, respectively, re-oxidized in one step with water or in two steps with water and air (Fig. 11). In the first case, the material appeared very active in methanol conversion, whereas in the second one, the initial catalytic behavior was very similar to that of the original, freshly calcined oxide [51]; in fact, the conversion was low, and then increased, at first slowly and then more rapidly. The high activity shown by the solid incompletely re-oxidized by water was due to the fact that the reduced oxide was more active than the fully oxidized spinel, as it appeared from results in Fig. 2.

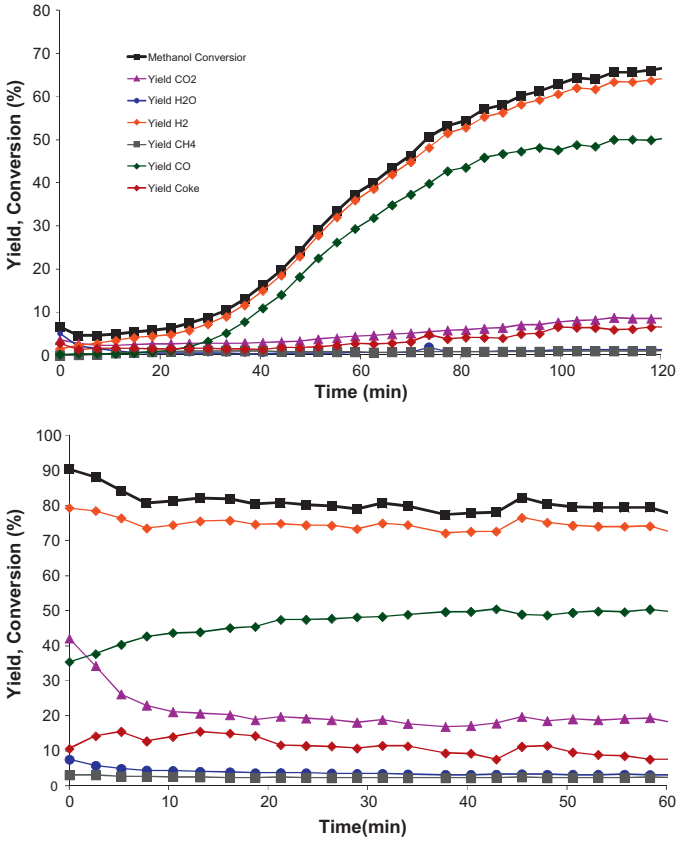

Fig. 11. CF450 2nd cycle of reduction, at 300 °C for two different materials (after the 1st complete RedOx cycle): (a) re-oxidation carried out with water and then air; (b) re-oxidation carried out with water only.

Fig. 12 summarizes the results obtained during 3 cycles, showing the evolution of initial methanol conversion registered during each reduction step of a CF450 sample, which was re-oxidized with either water only, or water and then air. It was shown that the initial activity of the spinel remained low all along the 3 cycles for the two steps (water and then air) re-oxidation: a behavior typically shown by the calcined and fully oxidized spinel. Conversely, the initial activity shown by the solid only partially re-oxidized during the 2nd and 3rd cycle was much higher than that shown by the freshly calcined spinel. It is also important to notice that the spinel, which had undergone 3 cycles, with only steam being used during the re-oxidation step, still contained a carbon content of 21.5 wt%, that clearly indicates the inefficiency of this procedure in removing the carbon deposits formed during the reduction step.

Even if a higher activity was observed in catalytic tests where air re-oxidation was not performed, a two-step re-oxidation may be preferred, since it led to the complete recovery of the original structure and to the formation of less coke; indeed coke deposition rate was lower in the first period of reduction of the starting spinel with methanol. It would also avoid or limit the formation of iron carbide, which may, in the end, cause a rearrangement of the material structure, and also avoid or limit the production of COx during the re-oxidation step with water, to obtain a high-quality hydrogen stream. Lastly, a third step of air re-oxidation of the material may lead to the complete removal of coke accumulation, when a considerable deposition takes place. The use of an only partially re-oxidized solid, where still residual coke is present, may limit the overall amount of hydrogen produced during the following re-oxidation step with steam.

Because of all these reasons, it is possible to conclude that the best approach to carry out the cycle reforming of methanol is:

(1) Use a short reduction time, in order to limit coke deposition on the solid and avoid deep modifications in the structure (for instance, carbide formation and sintering);
(2) Use a three-step approach (reduction, re-oxidation with water, and then with air), in order to (i) completely oxidize the residual coke still present after the water re-oxidation step, and (ii) recover the original oxidation state of the material, in order to limit coke deposition during the next reduction steps.

The procedure here described can be taken in consideration as a possible solution to overcome deactivation phenomena during repeated cycles.

4. Conclusions

In this work, we demonstrate the feasibility of a cyclic process simulating the steam-iron process, in which a $CoFe_2O_4$ spinel is used as an O^{2-} and electron carrier and methanol as the reducing agent. At first the cycle involved a deep reduction of the spinel, the latter having been calcined at either 450 or 750 °C, and a re-oxidation with steam of the reduced material. However, the characterization of the materials used demonstrated that the complete recovery of the original spinel phase is not possible when using this two-step approach. Conversely, it is possible to complete the cycle – that is, to recover the fully oxidized spinel phase – by adding a third step of re-oxidation by air. The material obtained after the three-step cycle also showed a reactivity behavior with regard to methanol, which was quite similar to that of the freshly calcined spinel. This demonstrates that a complete reconstruction of the spinel phase is possible even after a reduction step leading to the formation of both metallic species and Fe carbide compounds.

References

[1] G.A. Olah, Angew. Chem. Int. Ed. 117 (2005) 2692–2696.
[2] D.R. Palo, R.A. Dagle, J.D. Holladay, Chem. Rev. 107 (2007) 3992–4021.
[3] S. Sá, H. Silva, L. Brandão, J.M. Sousa, A. Mendes, Appl. Catal., B 99 (2010) 43–57.
[4] J.D. Holladay, J. Hu, D.L. King, Y. Wang, Catal. Today 139 (2009) 244–260.
[5] R.M. Navarro, M.A. Peña, J.L.G. Fierro, Chem. Rev. 107 (2007) 3952–3991.
[6] T. Kodama, N. Gokon, Chem. Rev. 107 (2007) 4048–4077.
[7] J.E. Funk, Int. J. Hydrogen Prod. 26 (2001) 185–190.
[8] T. Kodama, S. Miura, T. Shimizu, Y. Kitayama, Energy 22 (1997) 1019–1027.
[9] A. Steinfeld, P. Kuhn, J. Karni, Energy 18 (1993) 239–249.
[10] A. Steinfeld, A. Frey, P. Kuhn, D. Wuillemin, Int. J. Hydrogen Energy 20 (1995) 793–804.
[11] T. Kodama, H. Ohtake, S. Matsumoto, A. Aoki, T. Shimizu, Y. Kitayama, Energy 25 (2000) 411–425.
[12] P. Pantu, K. Kim, G.R. Gavalas, Appl. Catal., A 193 (2000) 203–214.
[13] K. Otsuka, Y. Wang, M. Nakamura, Appl. Catal., A 183 (1999) 317–324.
[14] M. Bohmer, U. Langnickel, M. Sanchez, Solar Energy Mater. 24 (1991) 441–448.
[15] O. Yokota, Y. Oku, T. Sano, N. Hasegawa, J. Matsunami, M. Tsuji, Y. Tamaura, Int. J. Hydrogen Energy 25 (2000) 81–86.
[16] P.B. Tarman, R. Biljetina, Coal Proc. Technol. 5 (1979) 114–116.
[17] H. Lane, The Lane Hydrogen Producer, 1909, Available online at ⟨http://www.flightglobal.com/pdfarchive/view/1909/1909%20-%200522.html⟩.
[18] A. Messerschmitt, German Patent DE 266863; 1911.
[19] T. Nakamura, Sol. Energy 19 (1977) 467–475.
[20] R. Villa, C. Cristiani, G. Groppi, L. Lietti, P. Forzatti, U. Cornaro, S. Rossini, J. Mol. Catal. A: Chem. 204–205 (2003) 637–646.
[21] P. Chiesa, G. Lozza, A. Malandrino, M. Romano, V. Piccolo, Int. J. Hydrogen Energy 33 (2008) 2233–2245.
[22] A. Pineau, N. Kanari, I. Gaballah, Thermochim. Acta 447 (2006) 89–100.
[23] K. Otsuka, C. Yamada, T. Kaburagi, S. Takenaka, Int. J. Hydrogen Energy 28 (2003) 335–342.
[24] K. Otsuka, A. Mito, S. Takenaka, I. Yamanaka, Int. J. Hydrogen Energy 26 (2001) 191–194.
[25] V. Galvita, T. Schröder, B. Munder, K. Sundmacher, Int. J. Hydrogen Energy 33 (2008) 1354–1360.
[26] S. Fukase, T. Suzuka, Appl. Catal., A 100 (1993) 1–17.
[27] V. Hacker, G. Faleschini, H. Fuchs, R. Fankhauser, G. Simader, M. Ghaemi, B. Spreitz, K. Friedrich, J. Power Sources 71 (1998) 226–230.
[28] V. Hacker, R. Fankhauser, G. Faleschini, H. Fuchs, K. Friedrich, M. Muhr, K. Kordesch, J. Power Sources 86 (2000) 531–535.
[29] V. Hacker, J. Power Sources 118 (2003) 311–314.
[30] S. Takenaka, K. Nomura, N. Hanaizumi, K. Otsuka, Appl. Catal., A 282 (2005) 333–341.
[31] S. Takenaka, N. Hanaizumi, V. Son, K. Otsuka, J. Catal. 228 (2004) 405–416.
[32] K. Matsuoka, T. Shimbori, K. Kuramoto, H. Hatano, Y. Suzuki, Energy Fuels 20 (2006) 2727–2731.
[33] M.F. Bleeker, S.R.A. Kersten, H.J. Veringa, Catal. Today 127 (2007) 278–290.
[34] M.F. Bleeker, S. Gorter, S.R.A. Kersten, L. van der Ham, H. van den Berg, H. Veringa, Clean Technol. Environ. Policy 12 (2010) 125–135.
[35] M.F. Bleeker, H.J. Veringa, S.R.A. Kersten, Ind. Eng. Chem. Res. 49 (2010) 53–64.
[36] M.F. Bleeker, H.J. Veringa, S.R.A. Kersten, Appl. Catal., A 357 (2009) 5–17.
[37] P. Heidebrecht, K. Sundmacher, Chem. Eng. Sci. 64 (2009) 5057–5065.
[38] K.-S. Go, S.-R. Son, S.-D. Kim, K.-S. Kang, C.-S. Park, Int. J. Hydrogen Energy 34 (2009) 1301–1309.
[39] E. Lorente, J.A. Peña, J. Herguido, Int. J. Hydrogen Energy 33 (2008) 615–626.
[40] E. Lorente, J.A. Peña, J. Herguido, J. Power Sources 192 (2009) 224–229.
[41] E. Lorente, J.A. Peña, J. Herguido, Int. J. Hydrogen Energy 36 (2011) 7043–7050.
[42] Z. Kang, Z.-L. Wang, Adv. Mater. 15 (2003) 521–526.
[43] E. Lorente, Q. Cai, J.A. Peña, J. Herguido, N.P. Brandon, Int. J. Hydrogen Energy 34 (2009) 5554–5562.
[44] C.C. Cormos, Int. J. Hydrogen Energy 35 (2010) 2278–2289.
[45] A. Steinfeld, P. Kuhn, A. Reller, R. Palumbo, J. Murray, Y. Tamaura, Int. J. Hydrogen Energy 23 (1998) 767–774.
[46] A. Steinfeld, M. Brack, A. Meier, A. Weidenkaff, D.A. Wuillemin, Energy 23 (1998) 803–814.
[47] T. Kodama, T. Shimizu, T. Satoh, M. Nakata, K.I. Shimizu, Sol. Energy 73 (2002) 363–374.
[48] K.-S. Kang, C.-H. Kim, W.-C. Cho, K.-K. Bae, S.-W. Woo, C.-S. Park, Int. J. Hydrogen Energy 33 (2008) 4560–4568.
[49] K.-S. Kang, C.-H. Kim, K.-K. Bae, W.-C. Cho, W.-J. Kim, Y.-H. Kim, S.-H. Kim, C.-S. Park, Int. J. Hydrogen Energy 35 (2010) 568–576.
[50] K.-S. Cha, H.-S. Kim, B.-K. Yoo, Y.-S. Lee, K.-S. Kang, C.-S. Park, Y.-H. Kim, Int. J. Hydrogen Energy 34 (2009) 1801–1808.
[51] V. Crocellà, F. Cavani, G. Cerrato, S. Cocchi, M. Comito, G. Magnacca, C. Morterra, J. Phys. Chem. C 116 (2012) 14998–15009.
[52] V.J. Aston, B.W. Evanko, A.W. Weimer, Int. J. Hydrogen Energy 38 (2013) 9085–9096.
[53] N. Ballarini, F. Cavani, S. Passeri, L. Pesaresi, A.F. Lee, K. Wilson, Appl. Catal., A 366 (2009) 184–192.
[54] J.M.M. Millet, C. Virely, M. Forissier, P. Bussière, J.C. Vedrine, Hyperfine Interact. 46 (1989) 619–628.
[55] I. Lima Junior, J.M.M. Millet, M. Aouine, M. do Carmo Rangel, Appl. Catal., A 283 (2005) 91–98.
[56] L. Zhang, J.M.M. Millet, U.S. Ozkan, J. Mol. Catal. A: Chem. 309 (2009) 63–70.
[57] H.H. Hamdeh, W.M. Hikal, S.M. Taher, J.C. Ho, N.P. Thuy, O.K. Quy, N. Hanh, J. Appl. Phys. 97 (2005) 0643101–0643104.
[58] G.A. Sawatzky, F. Van Der Woude, A.H. Morrish, Phys. Rev. 187 (1969) 747–757.
[59] G.A. Sawatzky, F. Van Der Woude, A.H. Morrish, J. Appl. Phys. 39 (1968) 1204–1205.
[60] G.A. Sawatzky, J.M.D. Coey, A.H. Morrish, J. Appl. Phys. 40 (1969) 1402–1403.
[61] R.D. Desautels, J. van Lierop, J.M. Cadogan, J. Phys. Conf. Ser.V 217 (2010) 012105.
[62] X. Li, C. Kutal, J. Alloys Compd. 349 (2003) 264–268.
[63] S.W. Lee, C.S. Kim, J. Magn. Magn. Mater. 303 (2006) e315–e317.
[64] T.A.S. Ferreira, J.C. Waerenborgh, M.H.R.M. Mendonça, M.R. Nunes, F.M. Costa, Solid State Sci. 5 (2003) 383–392.
[65] C.E. Johnson, M.S. Ridout, T.E. Cranshaw, Proc. Phys. Soc. 81 (1963) 1079–1090.
[66] B. Kniep, A. Constantinescu, D. Niemeier, K.D. Becker, Z. Anorg. Allg. Chem. 629 (2003) 1795–1804.
[67] S. Herreyre, P. Gadelle, P. Moral, J.M.M. Millet, J. Phys. Chem. Solids 58 (1997) 1539–1545.
[68] J. Zhang, A. Schneider, G. Inden, Corros. Sci. 45 (2003) 1329–1341.
[69] K. Mondal, H. Lorethova, E. Hippo, T. Wiltowski, S.B. Lalvani, Fuel Process. Technol. 86 (2004) 33–47.
[70] E. Park, O. Ostrovski, J. Zhang, S. Thomson, R. Howe, Metall. Mater. Trans. B 32 (2001) 839–845.